iScience

CellPress
OPEN ACCESS

Article

PPM1G promotes cell proliferation via modulating mutant GOF p53 protein expression in hepatocellular carcinoma

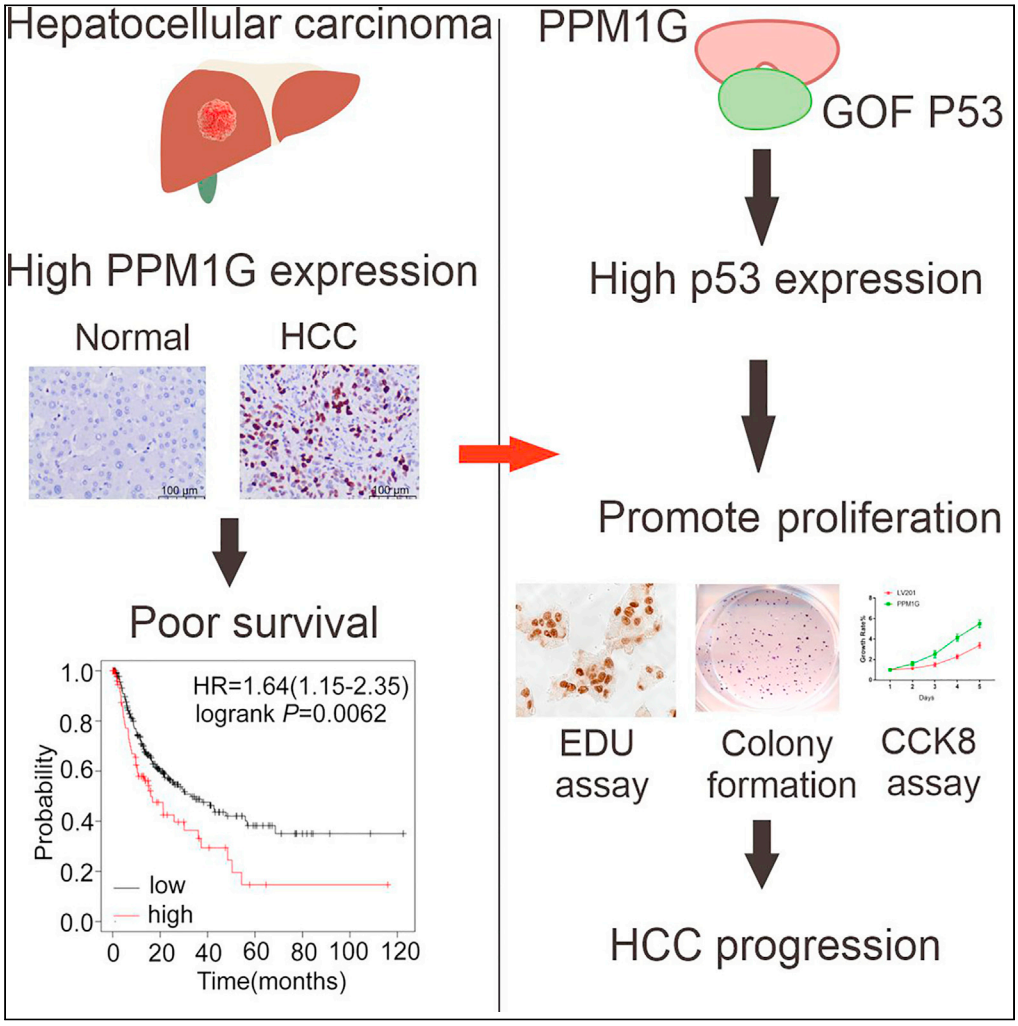

Wen Hu, Shao-Lin Ma, Liang Qiong, ..., Jian-Ning Chen, Xin-Yuan Guan, Chun-Kui Shao

chjning@mail.sysu.edu.cn (J.-N.C.)
xyguan@hku.hk (X.-Y.G.)
shaochk@mail.sysu.edu.cn (C.-K.S.)

Highlights

PPM1G is overexpressed in HCC tissues

High expression of PPM1G is associated with worse clinical outcomes

PPM1G promoted cell proliferation in *in vitro* and *in vivo* studies

PPM1G interacts with GOF mutant p53 protein and modulates its expression

Hu et al., iScience *27*, 109116
March 15, 2024
https://doi.org/10.1016/j.isci.2024.109116

iScience

CellPress
OPEN ACCESS

Article

PPM1G promotes cell proliferation via modulating mutant GOF p53 protein expression in hepatocellular carcinoma

Wen Hu,[1,7] Shao-Lin Ma,[2,7] Liang Qiong,[1] Yu Du,[1] Li-Ping Gong,[1] Yu-Hang Pan,[1] Li-Ping Sun,[1] Jing-Yun Wen,[6] Jian-Ning Chen,[1,*] Xin-Yuan Guan,[3,4,5,*] and Chun-Kui Shao[1,8,*]

SUMMARY

The serine/threonine protein phosphatase family involves series of cellular processes, such as pre-mRNA splicing. The function of one of its members, protein phosphatase, Mg^{2+}/Mn2+ dependent 1G (PPM1G), remains unclear in hepatocellular carcinoma (HCC). Our results demonstrated that PPM1G was significantly overexpressed in HCC cells and tumor tissues compared with the normal liver tissues at both protein and RNA levels. High PPM1G expression is associated with shorter overall survival ($p < 0.0001$) and disease-free survival ($p = 0.004$) in HCC patients. Enhanced expression of PPM1G increases the cell proliferation rate, and knockdown of PPM1G led to a significant reduction in tumor volume *in vivo*. Further experiments illustrated that upregulated-PPM1G expression increased the protein expression of gain-of-function (GOF) mutant p53. Besides, the immunoprecipitation analysis revealed a direct interaction between PPM1G and GOF mutant p53. Collectively, PPM1G can be a powerful prognostic predictor and potential drug-target molecule.

INTRODUCTION

With a global incidence of approximately 905,677 cases per year, hepatocellular carcinoma (HCC) represents the seventh most common malignancy and the second-leading cause of cancer-related death worldwide.[1] The vast majority (80–90%) of cases develops in patients with chronic liver disease or cirrhosis, and the main risk factors are viral hepatitis, alcohol intake, or metabolic syndrome, and non-alcoholic steatohepatitis associated with metabolic syndrome or diabetes mellitus is becoming a more frequent risk factor in the West.[2] Due to the rapid proliferation and high recurrence rate, the 5-year survival of patients with HCC is less than 30%, making it one of the most aggressive malignant tumors. The definitive diagnosis of HCC mainly relies on multiphase computed tomograpy (CT) and MRI with contrast.[3] A biopsy is warranted when image findings are highly suspicious but not diagnostic for HCC. Other approaches, such as liver ultrasonography and serum α fetoprotein level monitoring, are also considerable features when diagnosing HCC.[3] Artificial intelligence (AI) is now being explored for diagnosing HCC, although its clinical effect has not yet been validated.[4] Despite the wide use of advancing imaging systems, most patients were diagnosed with late-stage HCC diseases.[5] Surgical resection is appropriate for patients with early-stage disease without metastasis. For patients with advanced stages, percutaneous ablation, radiation, or chemotherapy can be applied. Liver transplantation is recognized as the most curable treatment option for patients with late-stage diseases, but the shortage of supplied liver organs limits its usage.[3] Recently, the combination of atezolizumab (anti-PDL1 monoclonal antibody) and bevacizumab (anti-VEGF monoclonal antibody) has been demonstrated as a promising therapeutic strategy for patients with advanced HCC with a moderate improvement in the survival time.[6] Still, it is urgent to identify key bio-markers and explicit mechanisms of HCC development to establish more efficient therapeutic strategies.

Protein serine/threonine phosphatases (PSPs) have been demonstrated to play crucial roles in cellular processes by cleaving phosphate from serine and threonine sites. Protein phosphatases are attractive therapeutic targets across numerous oncologic and non-oncologic indications. It has been categorized into three main families: (1) phosphoprotein phosphatases (PPPs), which include: protein phosphatase 1(PP1), PP2A, and PP2B; (2) metal-dependent protein phosphatases (PPMs), also represented by the type 2C protein phosphatases (PP2C); (3) aspartate-based phosphatases, including FCP1 and SCP1.[7] PPM1G (Mg2+/Mn2+-dependent protein phosphatase 1 gamma, also known as PP2Cγ) is a member of the PPMs family, which involves a variety of cellular signaling such as differentiation, proliferation,

[1]Department of Pathology, The Third Affiliated Hospital, Sun Yat-sen University, Guangzhou, Guangdong 510630, China
[2]Department of Gynecological Oncology, Sun Yat-sen Memorial Hospital, Sun Yat-sen University, Guangzhou, Guangdong 510120, China
[3]State Key Laboratory of Oncology in South China, Sun Yat-sen University Cancer Center, Guangzhou, Guangdong 510060, China
[4]Collaborative Innovation Center for Cancer Medicine, Sun Yat-sen University Cancer Center, Guangzhou, Guangdong 510060, China
[5]Department of Clinical Oncology, the University of Hong Kong, Hong Kong, China
[6]Department of Oncology, The Third Affiliated Hospital, Sun Yat-sen University, Guangzhou, Guangdong 510630, China
[7]These authors contributed equally
[8]Lead contact
*Correspondence: chjning@mail.sysu.edu.cn (J.-N.C.), xyguan@hku.hk (X.-Y.G.), shaochk@mail.sysu.edu.cn (C.-K.S.)
https://doi.org/10.1016/j.isci.2024.109116

survival, and metabolism.[8] Previous studies demonstrated that PPM1G modulates several nuclear functions, such as alternative splicing of specific pre-mRNAs, promoting spliceosome assembly,[9] and regulating the localization and stability of the survival motor neuron (SMN) complex.[10] Another study revealed the role of PPM1G in regulating protein translation and cell growth, which depends on the negative modulation of phosphorylation of 4E binding protein 1 (4E-BP1).[11] PPM1G also plays a crucial role in DNA damage responses by mediating the dephosphorylated forms of histone H2A and H2B.[12] Several studies investigated the expression and prognostic value of PPM1G in HCC,[13,14] but the detailed regulating mechanisms of PPM1G in the progression of HCC remain largely unexplored.

The TP53 gene is the second most frequently mutated gene in HCC, accounting for around 30% of all mutated genes.[15] The mutant p53 proteins can acquire new functions called gain-of-function (GOF) mutant p53 and play crucial roles in tumorigenesis. The E3 ubiquitin ligase MDM2 regulates the stability of p53 and contributes to HCC progression.[16] For example, some studies have shown that CDK9 inhibitors can enhance wild-type p53 stability and slow down the progression of HCC by interfering with MDM2 signaling.[17] However, the stability of GOF mutant p53 protein is enhanced in most human cancers, leading to its accumulation in the nucleus. Previous studies have demonstrated that TP53 mutations can cause aneuploid proliferation and chromosomal instability in liver cancer cells.[18] In addition, HCC patients with mutated TP53 exhibited advanced stages and had worse overall and relapse-free survival.[19] However, the underlying mechanisms of modulating GOF mutant p53 in HCC have not been fully elucidated thus far.

In the current study, we characterized the expression of PPM1G in fresh liver tissues using real-time PCR and western blot analysis and immunohistochemistry (IHC) in paraffin tissues. The correlation of PPM1G expression with various clinic-pathological characteristics and the prognosis predictive values in patients with HCC were also discussed. We also investigated the effects of PPM1G on cell proliferation and further detected the potential mechanisms. Our results indicated that PPM1G promotes HCC cell proliferation by increasing the protein expression of GOF mutant p53 protein.

RESULTS

PPM1G is overexpressed in HCC cell lines and tissues

We first evaluated the expression pattern of PPM1G in HCC. A real-time PCR analysis assay showed that the mRNA level of PPM1G was much higher in LM6, HEPG2, Huh7, and PLC8024 cells than in normal liver tissues (Figure 1A). The protein expression of PPM1G was also significantly increased in those four cell lines (Figure 1B). We further examined the expression pattern of PPM1G using fresh HCC tissues. We observed that both the mRNA and protein levels of PPM1G were elevated in tumor tissues compared to adjacent normal tissues (Figures 1C and 1D). Next, we determined the expression of PPM1G using a cohort of 96 patients with HCC from Sun Yat-sen University Cancer Center (SYSUCC). The IHC results showed that the PPM1G level was remarkably higher in tumor tissues than in the adjacent non-tumor tissues (Figure 1E, $p < 0.001$, Wilcoxon matched-paired test). To validate these results, we analyzed the expression of PPM1G in HCC using the The Cancer Genome Atlas Program (TCGA) dataset. We found overexpression of PPM1G in tumor tissues ($n = 369$) compared to normal tissues ($n = 160$) ($p < 0.05$) (Figure 1F). In addition, the transcripts per million in primary tumor tissues ($n = 371$) is also higher than in normal liver tissues according to the TCGA dataset (Figure 1G, $n = 50$, $p < 0.001$, Wilcoxon matched-paired test).[20] In short, our results demonstrated that PPM1G is overexpressed in HCC cells and tumor tissues.

High PPM1G expression is closely correlated with worse clinical outcomes

We next investigate the prognostic value of PPM1G in patients with HCC. We quantified the levels of PPM1G in tumor tissues and adjacent normal tissues by IHC staining in a cohort of 96 patients from SYSUCC. The information on clinical characteristics and clinical outcomes is presented in Table 1. In this cohort, the results revealed that the higher PPM1G expression was associated with advanced clinical characteristics, including elevated serum α-fetoprotein level ($p = 0.015$), advanced clinical stage ($p = 0.035$), poor differentiation ($p = 0.027$), more cancer embolus ($p = 0.022$), and tumor recurrence ($p = 0.015$) (Table 1). Importantly, PPM1G was shown to be an independent prognostic factor for overall survival (hazard ratio = 4.025; 95%CI: 2.015–8.037; $p < 0.0001$) (Tables 2 and 3). Moreover, Kaplan-Meier survival analysis suggested an unfavorable clinical outcome in patients with a higher level of PPM1G-expressing tumors (Figure 2A, overall survival, $p < 0.0001$; Figure 2B, disease-free survival, $p = 0.004$). From the TCGA project database, higher PPM1G expression is significantly associated with worse prognosis in patients with HCC compared to low PPM1G expression (Figure 2C, overall survival, $p = 9.3E-06$; Figure 2D, disease-free survival, $P = 5E-04$). These results indicated that PPM1G is a powerful predictive value for the clinical outcomes of HCC and a potential therapeutic target warranting further investigation.

PPM1G promotes HCC cell proliferation

To address the roles of PPM1G in HCC cells, we next examined its ability to regulate cell proliferation. We used lentivirus particles to transfect PPM1G-expressing plasmids or scrambled plasmids into PLC8024 and Huh7 cells with a relatively low PPM1G expression level. The overexpression efficiency of PPM1G was confirmed via western Blot and real-time PCR (Figure 3A). The colony formation assay revealed that the overexpressed cells exhibited a significantly higher proliferation rate than those with scrambled plasmids (Figure 3B). Meanwhile, the soft agar assay showed that the capacity of cells that are able to form colonies in an anchorage-independent manner was enhanced after the overexpression of PPM1G (Figure 3C). Furthermore, the EdU assay showed that cells with overexpressed PPM1G had improved proliferative ability (Figure 3D).

On the other hand, the proliferation rate can be abrogated when we knock down the expression of PPM1G in HCC cells (Figures S1A and 3B–3D). It is well known that cell migration would influence cell proliferation ability. Thus, we monitored cell migration after ectopic expression

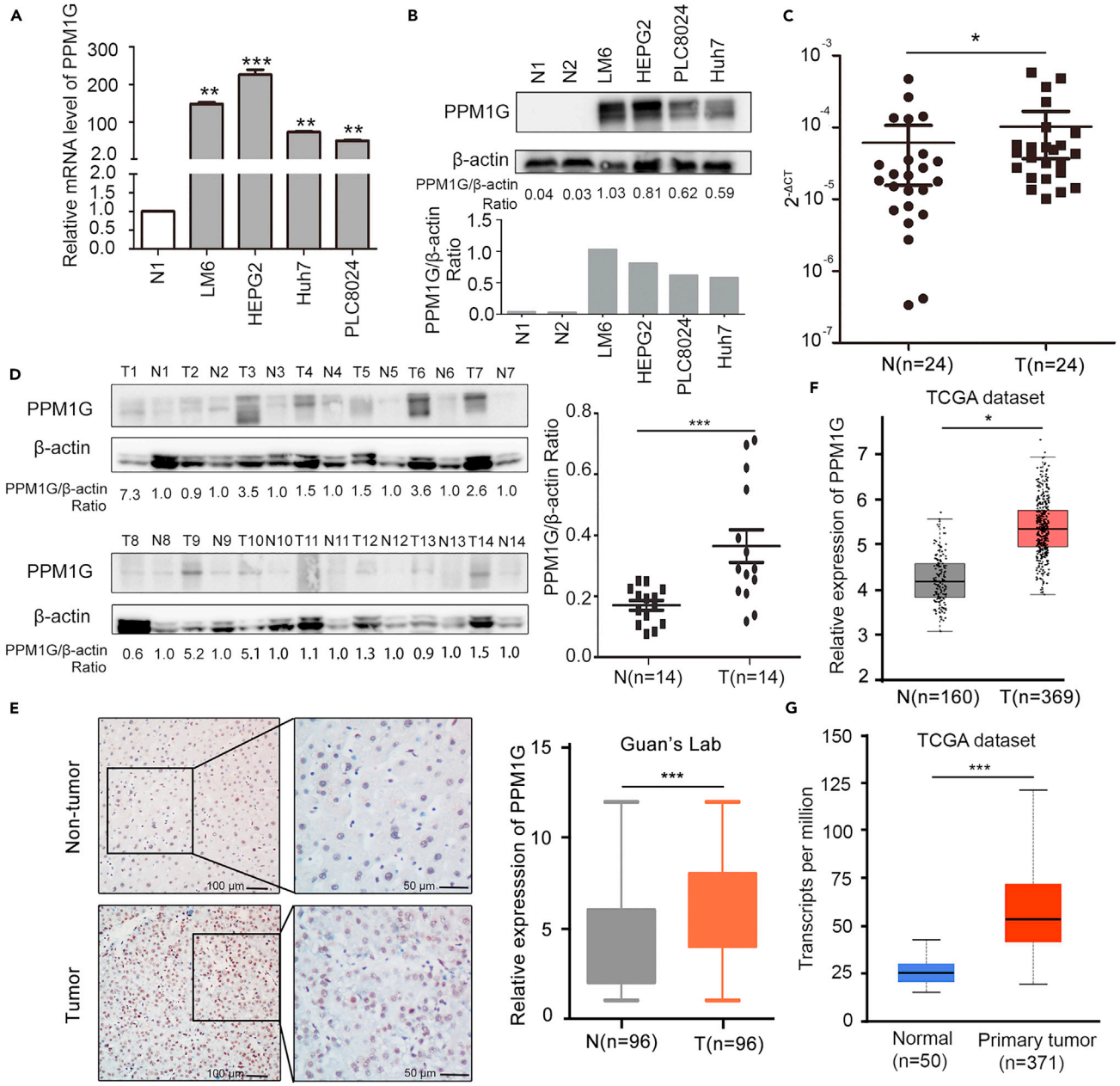

Figure 1. Expression of Mg2+/Mn2+-dependent protein phosphatase 1 gamma (PPM1G) in human HCC cells and tissues

(A) The HCC cell lines exhibited a higher level of PPM1G, as detected by real-time PCR, than fresh normal liver tissues. N1 refers to a normal liver tissue sample.

(B) The HCC cell lines exhibited a higher level of PPM1G expression, as detected by western blot, than fresh normal liver tissues. Both N1 and N2 refer to normal liver tissue samples (*$p < 0.05$, **$p < 0.01$, ***$p < 0.001$, t test). Normal liver tissue was used as a control.

(C) Real-time PCR showed that PPM1G was overexpressed in primary HCC tissues compared to adjacent nontumor liver tissues ($p < 0.05$, t test, $n = 24$). T, hepatocellular carcinoma tissue; N, non-tumor liver tissue.

(D) Western Blot showed that PPM1G was overexpressed in primary HCC tissues compared to adjacent non-tumor liver tissue. ($p < 0.001$, t test, $n = 14$). The ratio of PPM1G/β-actin of each group was shown.

(E) Immunohistochemistry showed strong staining of PPM1G in HCC. The adjacent non-neoplastic liver tissue expressed low PPM1G. The boxplot showed the mean staining intensity of PPM1G from HCC and normal liver tissue (HCC, $n = 96$; normal liver tissues, $n = 96$) ($p < 0.001$, Wilcoxon matched-paired test). Scale bar: left panel 100 μm, right panel 50 μm.

(F) PPM1G expression in TCGA HCC samples ($n = 369$) compared with unmatched non-tumor liver tissue (Wilcoxon matched-paired test, $n = 160$).

(G) Validation of PPM1G transcripts per million in TCGA HCC samples ($n = 371$) compared with unmatched normal liver tissue (Wilcoxon matched-paired test, $n = 50$). Data are represented as mean ± SD.

Table 1. Correlation of clinicopathological parameters and PPM1G expression (n = 96)

	PPM1G protein				
Variable	All cases	Low expression	High expression	x2	p value
Gender				0.066	0.591
female	2	2	4		
male	40	52	92		
Age (years)				0.034	0.552
≤60	32	42	74		
>60	10	12	22		
Tumor multiplicity				2.297	0.104
Single	37	41	78		
Multiple	5	13	18		
Tumor size (cm)				0.819	0.243
≤5	21	22	43		
>5	21	32	53		
HBsAg				1.198	0.224
yes	6	4	10		
no	36	50	86		
AFP (ng/ml)				5.600	0.015
<20	31	27	58		
≥20	11	27	38		
Differentiation				5.091	0.027
Well (I)	35	35	70		
Moderate (II)	3	4	7		
Poor/Undifferentiation (III/IV)	4	15	19		
Liver cirrhosis				1.996	0.138
yes	35	50	85		
no	7	4	11		
Cancer embolus				5.074	0.022
yes	2	11	13		
no	40	42	82		
TNM				4.075	0.035
I/II	31	29	60		
III/IV	11	25	36		
Relapse				5.873	0.015
yes	0	7	7		
no	42	47	89		
HBV DNA				3.388	0.052
yes	21	37	58		
no	21	17	38		

of PPM1G in HCC cells. Our results displayed that PPM1G can only slightly change cell migration (Figure S1B). Further study showed that in the mice model, PPM1G knockdown (PPM1G shRNA) significantly suppressed tumor growth after subcutaneously injected into the nude mice. The tumor regression was reflected in smaller tumor weight and tumor volume than the control (LVRU6GP) group (Figure 4).

PPM1G enhances the protein expression of GOF mutant p53 protein

To explore the underlying mechanisms of PPM1G modulating HCC proliferation, we performed protein-protein or protein-DNA binding analysis using online Ingenuity Pathways Analysis software (https://www.nihlibrary.nih.gov/resources/tools/ingenuity-pathways-analysis-ipa). We found several genes that can directly interact with PPM1G in protein or DNA levels, such as TP53, SNRNP70, TFAM, and MT-CO2 (Figure 5A).

Table 2. Univariate analysis of clinicopathological and PPM1G for overall survival and recurrence-free survival

	Overall survival		Recurrence-free survival	
Variable	HR (95% CI)	p value	HR (95% CI)	p value
Age (years)	0.723(0.319–1.639)	0.438	1.207(0.110–13.196)	0.877
Gender	1.695(0.205–14.023)	0.624	81924.529(0.00-∞)	0.984
HBsAg	3.655(0.441–30.276)	0.155	0.406(0.018–9.346)	0.573
AFP (ng/mL)	1.665(0.877–3.159)	0.119	0.321(0.032–3.175)	0.331
Liver cirrhosis	0.440(0.104–1.863)	0.265	0.000(0.000–4.84*10^{271})	0.975
Tumor size (cm)	1.996(0.995–4.003)	0.052	1.328(0.159–11.104)	0.793
Tumor multiplicity	0.834(0.398–1.748)	0.631	0.510(0.043–6.084)	0.594
Cancer embolus	5.172(2.104–12.711)	0.000	0.000(0.000-∞)	0.985
Differentiation	1.212(0.819–1.793)	0.337	1.113(0.476–2.605)	0.805
TNM stage	1.093(0.581–2.055)	0.782	4.066(0.658–25.112)	0.131
HBV DNA	0.627(0.326–1.208)	0.163	2.474(0.126–48.682)	0.551
PPM1G	3.691(1.685–8.081)	0.001	266876.046(0.0–7.54*10^{168})	0.948

TP53 has been widely reported as an essential factor in tumorigenesis, including HCC. In tumor cells, mutated TP53 can acquire new functions (GOFs) distinct from the wild-type one, significantly affecting cancer progression.[21] We then determined the expression level of GOF mutant p53 protein in PPM1G-overexpressed cells. As shown in Figure 5B, the GOF mutant p53 protein expression was increased in PPM1G-overexpressed cells. Meanwhile, the TCGA dataset also confirmed that the expression of PPM1G positively correlated with TP53 at the mRNA level (Figure 5B). Next, we performed co-immunoprecipitation assays to explore whether PPM1G and GOF mutant p53 interact directly. Our results demonstrated a direct interaction between PPM1G and GOF mutant p53 protein (Figure 5C), which might be one potential mechanism for which PPM1G regulated GOF mutant p53 protein expression.

DISCUSSION

The present study demonstrated that PPM1G was significantly upregulated in HCC tissues, and the overexpressed PPM1G could lead to enhanced proliferation in HCC cells and predict poor prognosis in HCC patients. PPM1G can also regulate tumor growth by modulating the protein expression of GOF mutant p53 via a direct interaction. Our findings have provided a better understanding of how the protein phosphatase regulates HCC progression and may have clinical implications in novel promising molecular targets for the therapeutic approach in patients with HCC.

For decades, serine/threonine protein phosphatase has been characterized as the crucial regulator in a variety of cellular functions in solid tumors. For instance, PP5 has been reported to be involved in MAPK-mediated cell growth and apoptosis, cell cycle, and DNA damage response.[22] It has been demonstrated that the protein phosphatase 2A (PP2A) regulatory subunit PR70 is a tumor suppressor gene in melanoma.[23] However, little is known about the roles of PPM1G in the development of HCC. Recently, several studies have reported that PPM1G is overexpressed in HCC, and high expression of PPM1G is associated with the progression and poor prognosis of HCC.[13,14] Besides, another research showed that PPM1G was highly expressed in lung adenocarcinoma (LUAD) cancer tissues. The high expression of PPM1G was associated with poor clinical stage, T stage, N stage, and overall survival in LUAD.[24] In the present study, we provided solid evidence to support that the overexpression of PPM1G is related to poorer survival in patients with HCC and could serve as a prognostic marker.

Wild-type TP53 is a well-known tumor suppressor gene that plays a crucial role in regulating tumor development. Mutated TP53 has been reported in many human cancers, and GOF mutant p53 can acquire new abilities to promote tumor development.[25] Many studies demonstrated that GOF mutant p53 was presented in HCC and involved in tumorigenesis. However, the mechanisms that regulate GOF mutant p53 expression remain unclear. Our results demonstrated that the knockdown of PPM1G can decrease p53 protein expression in HCC cells with GOF mutant p53. Previous studies have established that PPM1G can dephosphorylate USP7 and consequently lead to the degradation of Mdm2 as well as the degradation of p53.[26] Therefore, the disruption of USP7 and

Table 3. Multivariate analysis of clinicopathological and PPM1G for overall survival

	Overall survival	
Variable	HR (95% CI)	p value
Cancer embolus	5.544(2.570–11.958)	0.000
PPM1G	4.025(2.015–8.037)	0.000

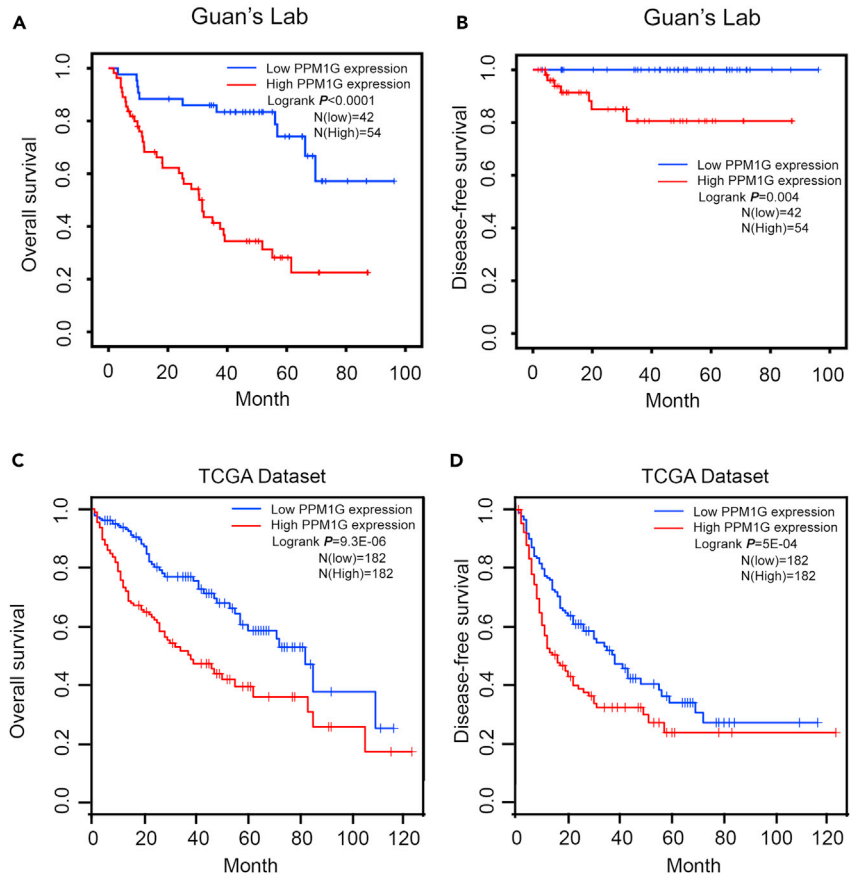

Figure 2. PPM1G overexpression has given rise to a poor prognosis of HCC

(A) Kaplan-Meier analyzed the correlation between PPM1G expression and the overall survival of HCC patients in SYSUCC (n = 96).

(B) Kaplan-Meier's analysis of the correlation between PPM1G expression and the disease-free survival of HCC patients in SYSUCC (n = 96).

(C) Overall survival analysis based on PPM1G expression levels in TCGA hepatocellular carcinoma tissues.

(D) Disease-free survival analysis based on PPM1G expression levels in TCGA HCC tissues.

Mdm2 phosphorylation caused the accumulation of p53. Pro-inflammatory cytokines, pro-oncogenic pathways, upfolded protein response (UPR) signaling, and autophagy form a positive feedback loop with mutant p53, which controls the stability of mutant p53 and tumor progression.[27] Future studies are warranted to explore whether the phosphorylation of USP7 and MDM2 contributes to the PPM1G-mediated GOF mutant p53 expression.

This study identified that overexpressed PPM1G in HCC can promote tumor development. Mechanistically, the PPM1G-mediated tumor progression was achieved by its direct interaction with GOF p53 proteins. Besides, plenty of studies have demonstrated that PPM1G plays multiple roles in tumor progression. For example, PPM1G is involved in immunosuppression by dephosphorylating stimulator of interferon genes (STING) or mitochondrial antiviral signaling protein (MAVS) proteins,[28] modulating spliceosome activities via alternative splicing,[29] and regulating cell migration or angiogenesis by phosphorylating SRSF3.[30] Thus, PPM1G exhibits a high potential to be druggable. In the past decades, accumulating evidence has shown that the pharmacological manipulation of phosphatase/diphosphatase activity by targeting serine/threonine phosphatases exhibits therapeutic benefits. Small molecular inhibitors, mono-antibodies, or antibody–drug conjugate (ADC) agents that target PPM1G all warrant further investigations in future studies. Given that PPM1G can interact with GOF p53, the therapeutic strategies that abrogate such interaction can be developed to inhibit tumor growth. Here, our observations provide a broad impact in understanding how PPM1G regulates the tumor progression in HCC as well as the underlying mechanisms. Taken together, our results supported that PPM1G can serve as a potential predictive marker for HCC prognosis and can be a future therapeutic target.

Limitations of the study

In this study, we have demonstrated that PPM1G can directly interact with GOF mutant p53 proteins. It is one potential mechanism that PPM1G regulated GOF p53 expression. Nonetheless, this study did not investigate the mechanisms by which PPM1G upregulates GOF p53 proteins.

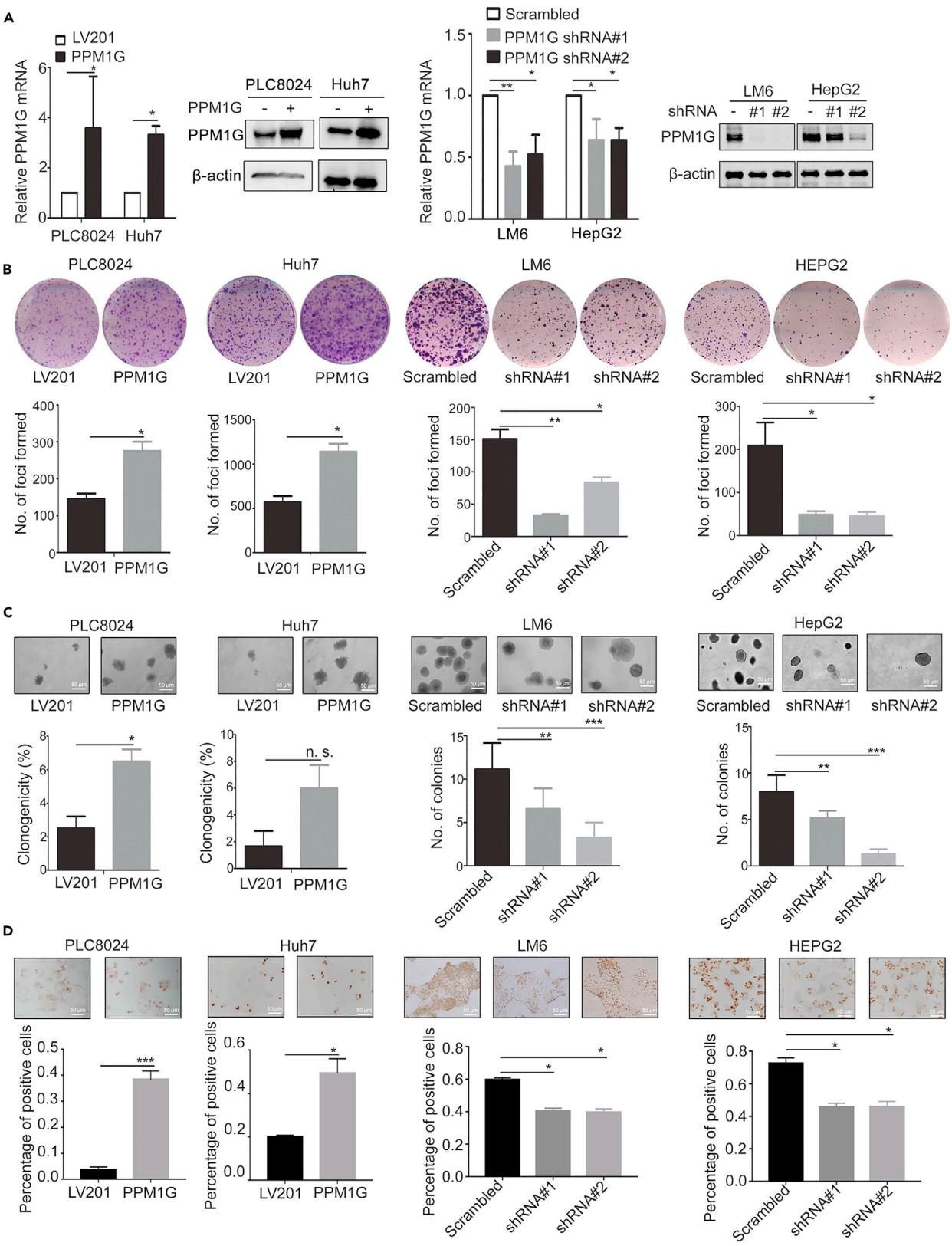
A
LV201
PPM1G
Relative PPM1G mRNA
PLC8024
Huh7
PPM1G
β-actin
Scrambled
PPM1G shRNA#1
PPM1G shRNA#2
LM6
HepG2
shRNA
#1 #2
B
PLC8024
Huh7
LM6
HEPG2
No. of foci formed
Scrambled
shRNA#1
shRNA#2
C
Clonogenicity (%)
n. s.
No. of colonies
D
Percentage of positive cells

Figure 3. Overexpressed PPM1G promotes HCC cell proliferation

(A) Cells stably transfected with PPM1G overexpressed plasmids, knockdown plasmids, or scrambled plasmids were verified by real-time PCR and western Blot.
(B) Overexpressed PPM1G enhanced the monoclonal formation ability of HCC cells. The ability of cell colony formation was detected by colony formation assay. The number of colonies was shown.
(C) Overexpressed PPM1G elevated the soft agar monoclonal formation ability of HCC cells. The number of colonies was shown. Scale bar: 50 μM.
(D) Overexpressed PPM1G enhanced HCC cell proliferation capacity, which was detected by EdU assay. Meanwhile, the PPM1G knockdown suppressed HCC cell proliferation capacity, which was detected by colony formation, soft agar, and EdU assay. Scale bar: 50 μM. All *p < 0.05, **p < 0.01, ***p < 0.001; t test. All experiments were performed in triplicate, and data are expressed as the mean of three samples with standard deviation.

STAR★METHODS

Detailed methods are provided in the online version of this paper and include the following:

- KEY RESOURCES TABLE
- RESOURCE AVAILABILITY
  - Lead contact
  - Materials availability
  - Data and code availability
- EXPERIMENTAL MODEL AND STUDY PARTICIPANT DETAILS
  - *In vivo* studies
  - Patients and specimens
  - Ethics approval statement
  - Informed consent
- METHOD DETAILS
  - Cell line and cell culture, plasmid and stable cell line generation
  - Western blot analysis
  - Cell viability assay
  - Colony formation assay and soft agar assay
  - EdU assay
  - Immunohistochemistry (IHC)
  - RNA extraction and real-time PCR
  - Co-immunoprecipitation assay
  - Image acquisition
- QUANTIFICATION AND STATISTICAL ANALYSIS

SUPPLEMENTAL INFORMATION

Supplemental information can be found online at https://doi.org/10.1016/j.isci.2024.109116.

ACKNOWLEDGMENTS

This work was supported by grants from the National Natural Science Foundation of China (82073397 and 82203263), the Guangdong Basic and Applied Basic Research Foundation (2022A1515012555, 2021A1515110979, and 2314050000259), the Medical Scientific Research

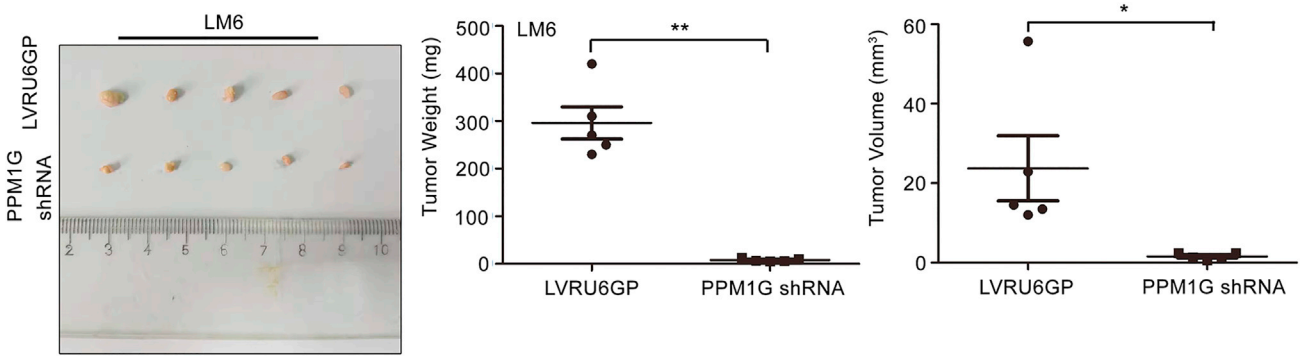

Figure 4. PPM1G knockdown inhibited tumor growth *in vivo*

Stable cell lines were subcutaneously injected into the flank of nude mice (n = 5). Tumors were sectioned on day 28. The tumor volumes were recorded every three days. The tumor size and tumor volume of the PPM1G knockdown (PPM1G shRNA) group were smaller than those of the control (LVRU6GP) group. All *p < 0.05, **p < 0.01, ***p < 0.001; t test. Data are represented as mean ± SD.

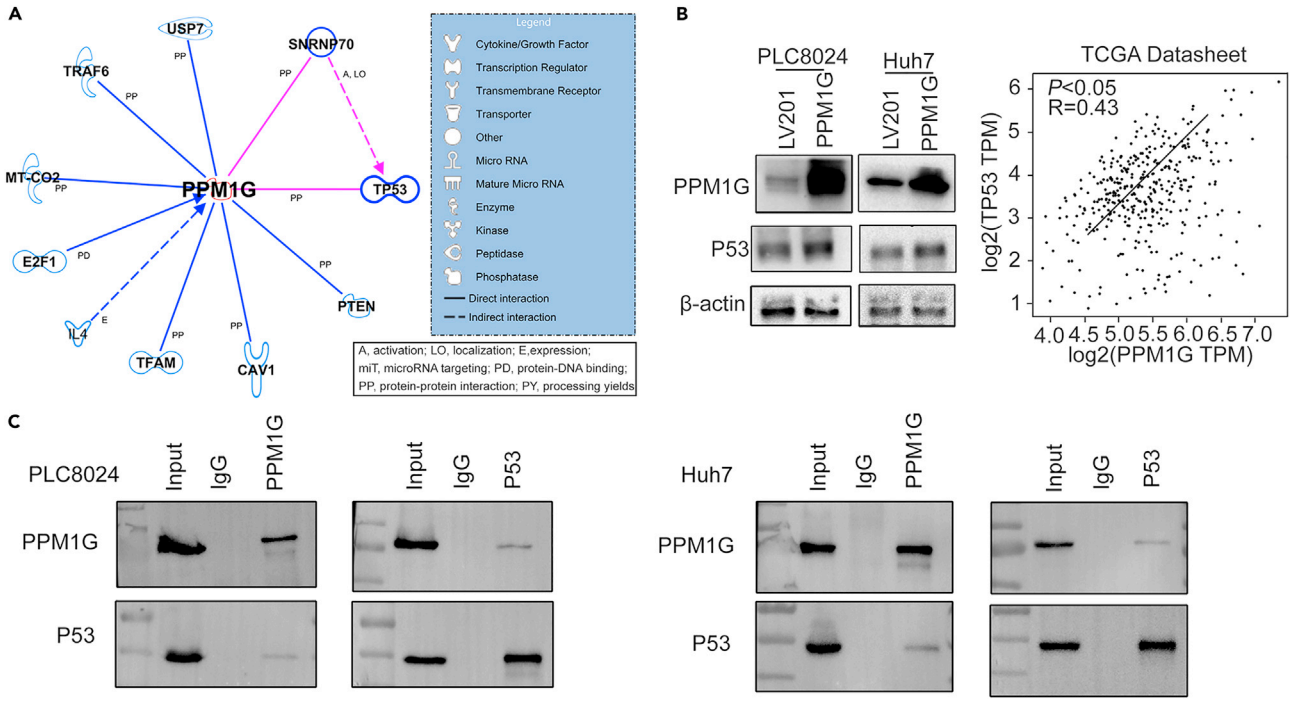

Figure 5. Overexpressed PPM1G enhanced GOF mutant p53 protein expression in HCC cell lines

(A) Online analysis tool IPA predicted that PPM1G and TP53 have protein-protein interaction.

(B) Overexpressed PPM1G increased GOF mutant p53 protein expression in PLC8024 and Huh7 cells. TCGA dataset showed that the mRNA level of PPM1G was positively correlated with TP53($R = 0.43$; $p < 0.05$).

(C) The coIP experiment showed a direct interaction between PPM1G and GOF mutant p53. Data are represented as mean ± SD.

Foundation of Guangdong Province, China (A2022017), the Guangzhou Science and Technology Project (202102010156 and 202102010141) and the China Postdoctoral Science Foundation (2022M713602) and the NSFC cultivating grant of The Third Affiliated Hospital, Sun Yat-sen University (2020GZRPYMS01), Guangdong Province, China. Thanks to the selfless help of Shao and Guan's lab, the strong support of the patients in this experiment, and the sacrifice of experimental animals for scientific inquiry.

AUTHOR CONTRIBUTIONS

Conceptualization, C.-K.S., X.-Y.G., J.-N.C., W.H., and S.-L.M.; methodology, W.H., Q.L., S.-L.M., Y.D., L.-P.G., Y.-H.P., L.-P.S., and J.-Y.W.; investigation, W.H., S.-L.M., and J.-Y.W.; writing – original draft, W.H. and S.-L.M.; writing – review & editing, W.H., S.-L.M., and J.-N.C.; funding acquisition, W.H., S.-L.M., J.-N.C., C.-K.S.; supervision, J.-N.C., X.-Y.G., and C.-K.S.

DECLARATION OF INTERESTS

The authors declare no competing of interest.

Received: September 1, 2023
Revised: November 25, 2023
Accepted: January 31, 2024
Published: February 5, 2024

REFERENCES

1. Sung, H., Ferlay, J., Siegel, R.L., Laversanne, M., Soerjomataram, I., Jemal, A., and Bray, F. (2021). Global Cancer Statistics 2020: GLOBOCAN Estimates of Incidence and Mortality Worldwide for 36 Cancers in 185 Countries. CA. Cancer J. Clin. *71*, 209–249.
2. Llovet, J.M., Kelley, R.K., Villanueva, A., Singal, A.G., Pikarsky, E., Roayaie, S., Lencioni, R., Koike, K., Zucman-Rossi, J., and Finn, R.S. (2021). Hepatocellular carcinoma. Nat. Rev. Dis. Primers *7*, 6.
3. Ganesan, P., and Kulik, L.M. (2023). Hepatocellular Carcinoma: New Developments. Clin. Liver Dis. *27*, 85–102.
4. Lacalamita, A., Serino, G., Pantaleo, E., Monaco, A., Amoroso, N., Bellantuono, L., Piccinno, E., Scalavino, V., Dituri, F., Tangaro, S., et al. (2023). Artificial Intelligence and Complex Network Approaches Reveal Potential Gene Biomarkers for Hepatocellular Carcinoma. Int. J. Mol. Sci. *24*, 15286.
5. Vogel, A., Meyer, T., Sapisochin, G., Salem, R., and Saborowski, A. (2022). Hepatocellular carcinoma. Lancet *400*, 1345–1362.

6. Cheng, A.L. (2021). Pursuing efficacious systemic therapy for hepatocellular carcinoma. Nat. Rev. Gastroenterol. Hepatol. *18*, 95–96.
7. Shi, Y. (2009). Serine/threonine phosphatases: mechanism through structure. Cell *139*, 468–484.
8. Lu, G., and Wang, Y. (2008). Functional diversity of mammalian type 2C protein phosphatase isoforms: new tales from an old family. Clin. Exp. Pharmacol. Physiol. *35*, 107–112.
9. Allemand, E., Hastings, M.L., Murray, M.V., Myers, M.P., and Krainer, A.R. (2007). Alternative splicing regulation by interaction of phosphatase PP2Cgamma with nucleic acid-binding protein YB-1. Nat. Struct. Mol. Biol. *14*, 630–638.
10. Petri, S., Grimmler, M., Over, S., Fischer, U., and Gruss, O.J. (2007). Dephosphorylation of survival motor neurons (SMN) by PPM1G/PP2Cgamma governs Cajal body localization and stability of the SMN complex. J. Cell Biol. *179*, 451–465.
11. Liu, J., Stevens, P.D., Eshleman, N.E., and Gao, T. (2013). Protein phosphatase PPM1G regulates protein translation and cell growth by dephosphorylating 4E binding protein 1 (4E-BP1). J. Biol. Chem. *288*, 23225–23233.
12. Kimura, H., Takizawa, N., Allemand, E., Hori, T., Iborra, F.J., Nozaki, N., Muraki, M., Hagiwara, M., Krainer, A.R., Fukagawa, T., and Okawa, K. (2006). A novel histone exchange factor, protein phosphatase 2Cgamma, mediates the exchange and dephosphorylation of H2A-H2B. J. Cell Biol. *175*, 389–400.
13. Lin, Y.R., Yang, W.J., and Yang, G.W. (2021). Prognostic and immunological potential of PPM1G in hepatocellular carcinoma. Aging (Albany NY) *13*, 12929–12954.
14. Xiong, D.L., Li, Q., Wang, H., Jin, W.L., Fan, X.M., and Ma, Y.Y. (2022). High expression of PPM1G is associated with the progression and poor prognosis of hepatocellular carcinoma. Cancer Biomark. *34*, 13–22.
15. Totoki, Y., Tatsuno, K., Covington, K.R., Ueda, H., Creighton, C.J., Kato, M., Tsuji, S., Donehower, L.A., Slagle, B.L., Nakamura, H., et al. (2014). Trans-ancestry mutational landscape of hepatocellular carcinoma genomes. Nat. Genet. *46*, 1267–1273.
16. Levine, A.J. (2020). p53: 800 million years of evolution and 40 years of discovery. Nat. Rev. Cancer *20*, 471–480.
17. Yao, J.Y., Xu, S., Sun, Y.N., Xu, Y., Guo, Q.L., and Wei, L.B. (2022). Novel CDK9 inhibitor oroxylin A promotes wild-type P53 stability and prevents hepatocellular carcinoma progression by disrupting both MDM2 and SIRT1 signaling. Acta Pharmacol. Sin. *43*, 1033–1045.
18. Rao, C.V., Asch, A.S., and Yamada, H.Y. (2017). Frequently mutated genes/pathways and genomic instability as prevention targets in liver cancer. Carcinogenesis *38*, 2–11.
19. Yuan, R.H., Jeng, Y.M., Chen, H.L., Lai, P.L., Pan, H.W., Hsieh, F.J., Lin, C.Y., Lee, P.H., and Hsu, H.C. (2006). Stathmin overexpression cooperates with p53 mutation and osteopontin overexpression, and is associated with tumour progression, early recurrence, and poor prognosis in hepatocellular carcinoma. J. Pathol. *209*, 549–558.
20. Chandrashekar, D.S., Bashel, B., Balasubramanya, S.A.H., Creighton, C.J., Ponce-Rodriguez, I., Chakravarthi, B.V.S.K., and Varambally, S. (2017). UALCAN: A Portal for Facilitating Tumor Subgroup Gene Expression and Survival Analyses. Neoplasia *19*, 649–658.
21. Brosh, R., and Rotter, V. (2009). When mutants gain new powers: news from the mutant p53 field. Nat. Rev. Cancer *9*, 701–713.
22. Kang, Y., Lee, J.H., Hoan, N.N., Sohn, H.M., Chang, I.Y., and You, H.J. (2009). Protein phosphatase 5 regulates the function of 53BP1 after neocarzinostatin-induced DNA damage. J. Biol. Chem. *284*, 9845–9853.
23. van Kempen, L.C.L., Redpath, M., Elchebly, M., Klein, K.O., Papadakis, A.I., Wilmott, J.S., Scolyer, R.A., Edqvist, P.H., Pontén, F., Schadendorf, D., et al. (2016). The protein phosphatase 2A regulatory subunit PR70 is a gonosomal melanoma tumor suppressor gene. Sci. Transl. Med. *8*, 369ra177.
24. Yin, R., Qu, L., Wang, Z., Tang, J., Gu, H., Wang, X., Yang, D., Du, P., and Dong, M. (2023). Prognostic and immunological potential of PPM1G in lung adenocarcinoma. Mol. Med. Rep. *28*, 156.
25. Ma, S., McGuire, M.H., Mangala, L.S., Lee, S., Stur, E., Hu, W., Bayraktar, E., Villar-Prados, A., Ivan, C., Wu, S.Y., et al. (2021). Gain-of-function p53 protein transferred via small extracellular vesicles promotes conversion of fibroblasts to a cancer-associated phenotype. Cell Rep. *34*, 108726.
26. Khoronenkova, S.V., Dianova, I.I., Ternette, N., Kessler, B.M., Parsons, J.L., and Dianov, G.L. (2012). ATM-dependent downregulation of USP7/HAUSP by PPM1G activates p53 response to DNA damage. Mol. Cell *45*, 801–813.
27. D'Orazi, G., Cordani, M., and Cirone, M. (2021). Oncogenic pathways activated by pro-inflammatory cytokines promote mutant p53 stability: clue for novel anticancer therapies. Cell. Mol. Life Sci. *78*, 1853–1860.
28. Yu, K., Tian, H., and Deng, H. (2020). PPM1G restricts innate immune signaling mediated by STING and MAVS and is hijacked by KSHV for immune evasion. Sci. Adv. *6*, eabd0276.
29. Murray, M.V., Kobayashi, R., and Krainer, A.R. (1999). The type 2C Ser/Thr phosphatase PP2Cgamma is a pre-mRNA splicing factor. Genes Dev. *13*, 87–97.
30. Chen, D., Zhao, Z., Chen, L., Li, Q., Zou, J., and Liu, S. (2021). PPM1G promotes the progression of hepatocellular carcinoma via phosphorylation regulation of alternative splicing protein SRSF3. Cell Death Dis. *12*, 722.
31. Zheng, Y.L., Li, L., Jia, Y.X., Zhang, B.Z., Li, J.C., Zhu, Y.H., Li, M.Q., He, J.Z., Zeng, T.T., Ban, X.J., et al. (2019). LINC01554-Mediated Glucose Metabolism Reprogramming Suppresses Tumorigenicity in Hepatocellular Carcinoma via Downregulating PKM2 Expression and Inhibiting Akt/mTOR Signaling Pathway. Theranostics *9*, 796–810.
32. Wang, X., Wang, J., Tsui, Y.M., Shi, C., Wang, Y., Zhang, X., Yan, Q., Chen, M., Jiang, C., Yuan, Y.F., et al. (2021). RALYL increases hepatocellular carcinoma stemness by sustaining the mRNA stability of TGF-β2. Nat. Commun. *12*, 1518.
33. Jiang, L., Yan, Q., Fang, S., Liu, M., Li, Y., Yuan, Y.F., Li, Y., Zhu, Y., Qi, J., Yang, X., et al. (2017). Calcium-binding protein 39 promotes hepatocellular carcinoma growth and metastasis by activating extracellular signal-regulated kinase signaling pathway. Hepatology *66*, 1529–1545.
34. Li, Y., Chen, L., Chan, T.H.M., Liu, M., Kong, K.L., Qiu, J.L., Li, Y., Yuan, Y.F., and Guan, X.Y. (2013). SPOCK1 is regulated by CHD1L and blocks apoptosis and promotes HCC cell invasiveness and metastasis in mice. Gastroenterology *144*, 179–191.e4.
35. Guzmán, C., Bagga, M., Kaur, A., Westermarck, J., and Abankwa, D. (2014). ColonyArea: an ImageJ plugin to automatically quantify colony formation in clonogenic assays. PLoS One *9*, e92444.

STAR★METHODS

KEY RESOURCES TABLE

REAGENT or RESOURCE	SOURCE	IDENTIFIER
Antibodies		
Rabbit anti-human PPM1G	Abcam	Cat. #ab70794; RRID: AB_2170200
β-Actin (8H10D10) Mouse mAb	Cell Signaling Technology	Cat. #3700; RRID:AB_2242334
Mouse anti-human P53	Santa Cruz	Cat. #sc-126; RRID:AB_628082
GAPDH (D16H11) XP Rabbit mAb	Cell Signaling Technology	Cat. #5174; RRID:AB_10622025
Bacterial and virus strains		
Stbl3 competent cells	Genecopoeia	U01030A
Biological samples		
The formaldehyde-fixed and paraffin embedded tissues of HCC patients	SYSUCC	N/A
The fresh tissue of HCC patients	SYSUCC	N/A
Chemicals, peptides, and recombinant proteins		
Tris base	Sangon Biotech	A501492-0005
Non-fat powder milk	Sangon Biotech	A600669-0250
Glycine	Sangon Biotech	A502065-0005
NP-40	Sigma-Aldrich	Cat. #74385
TRIZOL Reagent	Life	Cat. #15596026
Tissue Freezing Medium	NCM Biotech	Cat. No:C40100
Phospho-Protease Inhibitor	Roche	Cat. #04906837001
Protease Inhibitor	Roche	Cat. #05892791001
Triton X-100	ZSGB-Bio	ZLI-9308
Penicillin Sterptomycin	Gibco	Cat. #15140122
Antifade Fluorescence Mounting Medium-Aqueous,Fluoroshield	Abcam	Cat. #ab104135
Cell lysis buffer for Western and IP	Beyotime	Cat No. P0013
Trypsin-EDTA Solution with phenol red	Biosharp	Cat. #BL512A
Sea plaque® Agarose	Lonza	Cat. #50100
SDS	Diamond	A100227-0500
Tween 20	Diamond	A100777-0500
Isopropanol	Sangon Biotech	A507048-0500
Crystal violet	MBCHEM	CAS#:548-62-9
DMEM medium	GIBCO	C11995500BT
Fetal Bovine Serum	Ex Cell Bio	Cat. No:FSP500
PBS PH7.4 basic (1x)	gibco	REF C10010500BT
Critical commercial assays		
Pierce™ IP/Co-IP kit	Thermo Fisher	Cat. #88804
Lipofectamine® 3000 Reagent	Invitrogen	Lot No.2079400
Enhanced BCA Protein Assay Kit	Beyotime	Cat No.P0009
Evo M-MLV RT Kit with gDNA Clean for qPCR	Accurate Biology	Cat. #AG11705
SYBR Green Premix Pro Taq H.S. qPCR kit	Accurate Biology	Cat. #AG11701
Beyoclick EdU cell proliferation kit with DAB	Beyotime	Cat No.C0085s

(*Continued on next page*)

Continued

REAGENT or RESOURCE	SOURCE	IDENTIFIER
Cell Counting Kit-8	Dojndo	Cat. #CK04-500T
ViraPower™ Lentiviral Packaging Mix	Thermo Fisher Scientific	Cat No. K497500
Lightning Chemiluminescence Reagent	Merck millipore	Cat. #WBKLS0100
MycoAlert® Mycoplasma Detection Kit	Lonza	Catalog #: LT07-418
Experimental models: Cell lines		
PLC8024	The Institute of Virology, Chinese Academy of Medical Sciences (Beijing, China)	N/A
HUH7	The Institute of Virology, Chinese Academy of Medical Sciences (Beijing, China)	N/A
HEPG2	The Institute of Virology, Chinese Academy of Medical Sciences (Beijing, China)	N/A
LM6	The Institute of Virology, Chinese Academy of Medical Sciences (Beijing, China)	N/A
Experimental models: Organisms/strains		
BALB/c Nude mice	Guangdong Medical Laboratory Animal Center	N/A
Oligonucleotides		
Primers for qRT-PCR		
PPM1G-FORWARD	Invitrogen	GCCAGCCGTGATGAAAATGGG
PPM1G-REVERSE	Invitrogen	TCGGGGCTTGAAGCAAATGA
18S-FORWARD	Invitrogen	CGCCGCTAGAGGTGAAATTC
18S-REVERSE	Invitrogen	TTGGCAAATGCTTTCGCTC
Recombinant DNA		
LV201	GeneCopoeia	EX-NEG-Lv201
PPM1G-LV201	GeneCopoeia	M0225
LVRU6GP	GeneCopoeia	CSHCTR001-LVRU6GP
PPM1G shRNA 31	GeneCopoeia	HSH058951-LVRU6GP
PPM1G shRNA 33	GeneCopoeia	HSH058951-LVRU6GP
Software and algorithms		
Prism version 8.00	GraphPad Software	https://www.graphpad.com/
ImageJ	NIH Image	https://imagej.nih.gov/ij/index.html
Online Ingenuity Pathways Analysis software	N/A	https://www.nihlibrary.nih.gov/resources/tools/ingenuity-pathways-analysis-ipa
SPSS 16.0	N/A	https://spss.software.informer.com/16.0/
Other		
fluorescence microscope	Nikon Eclipse 80i	N/A
Chemiluminescence Apparatus	CLINX	N/A
Microplate Reader	SYNERGY-HTX multi-mode reader	N/A

N/A, not available. SYSUCC: Sun Yat-sen University Cancer Center.

RESOURCE AVAILABILITY

Lead contact

Further information and requests for all original resources and reagents presented in this manuscript should be directed to the Lead Contact, Chun-Kui Shao (shaochk@mail.sysu.edu.cn).

Materials availability

There are no unique/stable reagents generated in this study.

Data and code availability

All data reported in this paper will be shared by the lead contact upon request. This paper does not report the original code. Any additional information required to reanalyze the data reported in this paper is available from the lead contact upon request.

EXPERIMENTAL MODEL AND STUDY PARTICIPANT DETAILS

In vivo studies

Male athymic nude mice (4–6 weeks of age, 18–22 g of body weight; 5 mice in each group) were obtained from the Guangdong Medical Laboratory Animal Center. All mice were raised in a specific pathogen-free environment 1–2 weeks before the experiment. All animal procedures were approved by the Institutional Animal Care and Use Committee at The third affiliated hospital of Sun Yat-sen University.[31,32] Briefly, mice have subcutaneously injected $5*10^6$ LM6 LVRU6GP (shCtrl) cells into the right beneath the flank of mice and $5*10^6$ LM6 PPM1G shRNA(shPPM1G) cells into the opposite flank of the same mice. After 4 weeks, the tumor volume was calculated based on the length (L) and the width (W) of the tumors with the formula $V = (L*W^2)/2$. Finally, all mice were euthanized by CO2 exposure, followed by a cervical dislocation. All the tumors from different groups were harvested and measured in weight.

Patients and specimens

A total of 96 paraffin-embedded primary liver cancer tissues and their corresponding non-tumor tissues were collected by the pathology department of Sun Yat-sen University Cancer Center from HCC patients who underwent a hepatectomy resection between December 2012 and January 2015 at this hospital. The written informed consent for the usage of clinical specimens for medical research was obtained from all patients. The histopathological diagnosis was double-blind and confirmed by two expert pathologists from Sun Yat-sen University Cancer Center (Guangzhou, China). All human samples presented in this study were approved by the Institute Research Medical Ethics Committee of Sun Yat-sen University.

Ethics approval statement

All animal procedures were approved by the Institutional Animal Care and Use Committee of Sun Yat-sen University. All human samples presented in this study were approved by the Institute Research Medical Ethics Committee of Sun Yat-sen University. All animal studies were done in randomization and single-blinded way.

Informed consent

Written informed consent was obtained from each patient.

METHOD DETAILS

Cell line and cell culture, plasmid and stable cell line generation

The HCC cell lines PLC8024 (*TP53*^{R249S}), Huh7 (*TP53*$^{Y22\circ C}$), LM6 (*TP53*^{E51}-Nonsense), and HepG2 (*TP53* wild-type) were used in this study, and their background information has been described in previous studies.[33,34] All cell lines were routinely tested for mycoplasma contamination and cultured with Dulbecco's modified Eagle's medium supplemented with 10% fetal bovine serum and 1% penicillin/streptomycin at 37°C under 5% CO_2 condition. Cell line authentication has been done by short tandem repeat (STR) profiling. The LV201, PPM1G-LV201, LVRU6GP, and PPM1G shRNA plasmids were purchased from GeneCopoeia. We did the lentiviral transfection with ViraPower Lentiviral Packaging Mix. The virus-containing supernatants were produced following the description. Then, the old medium was replaced with fresh medium containing 6 μg/mL polybrene and the virus suspension and incubated at 37°C for 4 h. About 2 mL of fresh medium was added to dilute polybrene, and the cells were used for further experiments within 48 h after transfection. The LV201 or PPM1G shRNA group was established using the lentivirus infection. The LV201 was used as a positive control. The selective medium containing puromycin (LV201 plasmids andPPM1G shRNA plasmids) was used to select the stably transfected monoclonal cell lines.

Western blot analysis

Briefly, cells were washed with ice-cold PBS, and tissues were ground by Liquid nitrogen, harvested, and lysed by ice-cold RIPA buffer containing 1:100 protease/phosphatase inhibitor cocktail. The BCA protein assay kit was used to measure the protein concentration. An equal amount of protein (30 μg) was loaded onto SDS-PAGE gels and transferred to PVDF membrane. Then, the membranes were blocked with 5% non-fat milk buffer for 1 h at room temperature, followed by the incubation with primary antibody overnight at 4°C. The next day, the membranes were washed thrice with TBST for 45 min and incubated with Horseradish Peroxidase (HRP)-linked secondary antibodies for 1 h at room temperature. After rinsing 3 times with TBST for 45 min, the western Lightning Chemiluminescence Reagent was added and exposed to the membrane with the Chemiluminescence Apparatus. The primary antibodies were listed in the key resources table: PPM1G, P53,β-actin et al. β-actin was used as the loading control.

Cell viability assay

Cells were harvested and seeded into 96-well plates with a number of 3000 per well. The cell viability was assessed using Cell Counting Kit-8 according to the manufacturer's instructions. Cells were incubated with the Cell Counting Kit-8 for 2.5h and measured by a Microplate reader at the wavelength of 490nm.

Colony formation assay and soft agar assay

The stable HCC cells were plated in a 6-well plate (1000 cells/dish) and cultured for 14 days for colony formation. The colonies were fixed with 75% ethanol for 15 min and stained with 0.1% crystal violet for 20 min. The colonies were counted using ImageJ software.[35] Agarose colony formation assay was carried out by splitting 3000 cells in 0.35% bactoagar on top of 0.5% base agar. Colonies were counted under a phase-contrast microscope after 3–4 weeks incubated at 37°C and 5% CO2 humidified incubator.

EdU assay

For the EdU assay, the transfected cells were cultured in the confocal dishes ($6*10^4$ cells/dish). Samples were fixed with 4% paraformaldehyde and then processed with Triton (1%) to perforate cell membranes for 5 min. Next, cells were incubated with EdU staining reagent for 30 min. Finally, a fluorescent microscope as instructed, was used to capture the image. Experiments were performed three times.

Immunohistochemistry (IHC)

A total of 96 paraffin-embedded HCC tissues and adjacent normal tissues were collected and cut into 3–5 μm sections. The sections were heated at 65°C for 60 min and followed by deparaffinization and hybridization with xylene and graded alcohols, respectively. Antigen retrieval was performed with EDTA buffer for 2 min 30 s in a pressure cooker for each slide. Then, the slides were incubated with 3% H2O2 for 15 min at room temperature. Nonspecific binding was blocked by incubating tissue sections with a blocking buffer for 1 h at room temperature. The primary antibody was applied for each slide and incubated at 4°C overnight. Then, each tissue section was rinsed with PBS thrice for 5 min each and HRP-conjugated anti-rabbit secondary antibody for 30 min at room temperature. After washing three times with PBS, the slides were incubated with DAB for 1 min. Finally, the slides were counterstained with hematoxylin for 15 s, PBS for 1 min, and mounted with the medium for microscope observation.

The expression of PPM1G in paraffin slides was assessed by the Semi-quantitative method based on the positive percentage and staining intensity. The positive percentage was evaluated with a score of "0" indicating less than 5% of positive cells, "1" indicating 6–24% of positive cells, "2" indicating 25–49% of positive cells, "3" indicating 50–74% of positive cells, and "4" indicating 75%–100% of positive cells. The score of intensity was determined as follows: "0" negative staining, "1" weak staining, "2" moderate staining, and "3" strong staining. The final numerical score was calculated by multiplying the positive percentage score with the staining intensity score. The cut-off score for defining high and low expression was 3. The immunohistochemistry score was double-blind, confirmed by two subspecialists from Sun Yat-sen University Cancer Center (Guangzhou, China). A third subspecialist reassessed the slides when there were discordances between the first 2 subspecialists.

RNA extraction and real-time PCR

Briefly, cell pellets or tissue samples were collected and resuspended in 1mL of TRIZOL reagent. Then, collect the supernatant by centrifugation (12 000 g, 10 min, 4°C), followed by adding 200 μL of chloroform and incubating at room temperature for 5 min. Then, add 600 μL of 2-propanol into the supernatant (600 μL) and culture for 10 min at room temperature and centrifuge at 12 000g for 10 min. Eventually, the RNA pellet was washed with 1 mL of 70% ethanol and dried at room temperature. Then, the transparent pellet was resuspended in 20 μL of Milli-Q water. According to the instruction, the total RNA (1 μg) was reversely transcribed into cDNA using High capacity cDNA Reverse Transcription Kit. PPM1G mRNA presented in the cells or tissues was determined by Universal SYBR Green quantitative real-time PCR assay (Taqman 2× Universal Master Mix with No AmpErase UNG). The reactions were run as follows: Initial denaturation for 10 min at 94°C, followed by 30 cycles with denaturation for 15 s at 94°C, annealing, and extension for 60 s at 60°C. The primers for PPM1G were used to determine the mRNA level of PPM1G. 18s rRNA was used as the endogenous control. The $2^{-\Delta\Delta CT}$ method was used to calculate the relative amount.

Co-immunoprecipitation assay

In the co-immunoprecipitation (co-IP) assay, cellular proteins were extracted using the lysis buffer from the Pierce IP/Co-IP kit, supplemented with a protease inhibitor cocktail. Following a 10-min centrifugation at 12 000 rpm to remove the cytoskeleton, the supernatant was incubated overnight at 4°C with either a specific primary antibody or a control rabbit/mouse IgG., Protein A/G beads from the Pierce IP/Co-IP kit were added to capture the antibody-protein complexes and incubated at room temperature for 1 h. The complexes were then collected using magnets. Subsequently, the antibody-protein-bead complexes were washed three times with the lysis/wash buffer. The elution buffer was used to release the proteins bound to the beads. Finally, the eluted proteins were denatured for western blotting analysis. A total of 10 μg whole-cell lysates were used as an input control.

Image acquisition

All images were examined with a Nikon Eclipse 80i microscope and captured with NIS-Elements F 3.2 imaging analysis system in normal bright-field mode. Images were saved as 8-bit TIFFs along with a scale bar. We use the autoexposure time with a gain of 1.0.

QUANTIFICATION AND STATISTICAL ANALYSIS

The differences were assessed by two-tailed Student's t-test for parametric data, and Wilcoxon signed rank, Kruskal-Wallis, or Mann Whitney test for non-parametric data. The statistical evaluation of this study was performed with SPSS16.0 (SPSS Inc., Chicago, IL, USA) and GraphPad Prism 8.0 (La Jolla, CA, USA). All results were described as means $\pm$ standard deviation of the mean (S.D.). Unless otherwise indicated, statistical significance was marked as *$p < 0.05$, **$p < 0.01$, and ***$p < 0.001$.